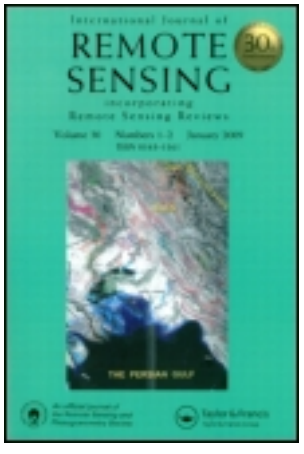

International Journal of Remote Sensing

Publication details, including instructions for authors and subscription information:
http://www.tandfonline.com/loi/tres20

Satellite remote sensing of dust aerosol indirect effects on cloud formation over Eastern Asia

S. C. Ou [a], K. N. Liou [a], N. C. Hsu [b] & S. C. Tsay [b]

[a] Joint Institute for Regional Earth System Science and Engineering, Department of Atmospheric and Oceanic Sciences, University of California, Los Angeles, CA, 90095, USA

[b] Climate and Radiation Branch, NASA Goddard Space Flight Center, Greenbelt, MD, 20771, USA

Version of record first published: 11 Jul 2012

To cite this article: S. C. Ou, K. N. Liou, N. C. Hsu & S. C. Tsay (2012): Satellite remote sensing of dust aerosol indirect effects on cloud formation over Eastern Asia, International Journal of Remote Sensing, 33:22, 7257-7272

To link to this article: http://dx.doi.org/10.1080/01431161.2012.700135

International Journal of Remote Sensing
Vol. 33, No. 22, 20 November 2012, 7257–7272

Taylor & Francis
Taylor & Francis Group

Satellite remote sensing of dust aerosol indirect effects on cloud formation over Eastern Asia

S. C. OU*†, K. N. LIOU†, N. C. HSU‡ and S. C. TSAY‡

†Joint Institute for Regional Earth System Science and Engineering, Department of Atmospheric and Oceanic Sciences, University of California, Los Angeles, CA 90095, USA

‡Climate and Radiation Branch, NASA Goddard Space Flight Center, Greenbelt, MD 20771, USA

(*Received 15 September 2011; in final form 16 April 2012*)

The dust aerosol indirect effect of the first kind on ice and liquid water cloud formation has been investigated using available MODIS cloud and aerosol products on the basis of correlation analysis. The variability in the correlation between cloud parameters, including optical depth, effective particle size, cloud water path and cloud particle number concentration, and aerosol variables, including optical depth and number concentration, over Eastern Asia has been studied. Three MODIS scenes that contain a significant presence of local and transported dust and clouds have been selected for comprehensive analysis. For all cases studied, we demonstrate that there is a negative trend regarding the correlation between cloud particle size and aerosol optical depth, which is statistically significant. These results represent a strong evidence of dust and cloud interactions that are consistent with the hypothesis of the Twomey effect for clouds.

1. Introduction

Atmospheric aerosols include mineral dust particles, organic suspensions and inorganic particles injected by biomass burning and wild fires and haze particles associated with urban air pollution. Among these particles, mineral dust is an important source of aerosols, which are lifted by dust storms from desert surfaces and transported across continents and oceans by atmospheric general circulation. These dust aerosols are often present over Africa, the equatorial Atlantic Ocean, the Middle East, South Asia, Northern China and the Northwest Pacific Ocean (Forster *et al.* 2007). Interactions between dust aerosols and clouds in the upper troposphere and lower stratosphere can produce a significant impact on atmospheric radiation budget, and hence on global and regional climates. By means of absorption and scattering processes, dust aerosols affect atmospheric radiative transfer through their direct interaction with solar and thermal infrared radiation. Dust aerosols also affect atmospheric radiative and climate forcings indirectly through their interaction with clouds by modifying cloud optical properties and precipitation efficiency. The direct aerosol radiative effect is much smaller than the direct cloud radiative effect. However, the aerosol indirect

*Corresponding author. Email: ssou@atmos.ucla.edu

International Journal of Remote Sensing
ISSN 0143-1161 print/ISSN 1366-5901 online © 2012 Taylor & Francis
http://www.tandfonline.com
http://dx.doi.org/10.1080/01431161.2012.700135

effects (AIEs) on cloud formation and the coupled modifications on radiative transfer and hydrological cycle can be significant processes in the atmosphere, albeit with large uncertainties.

The AIE of the first kind is commonly known as the 'Twomey effect' (Twomey 1977), an effect involving increases in the solar cloud albedo due to decreases in the cloud particle size caused by additional aerosols serving as cloud condensation nuclei (CCN) and ice nuclei (IN). Other types of indirect effects have also been identified and are referred to as the AIE of the second kind, including the effect on cloud lifetime and precipitation efficiency associated with additional smaller cloud particles (Liou and Ou 1989, Albrecht 1989), the solar absorption effect of soot particles related to decreases in precipitation efficiency (Grassl 1979, Hansen *et al.* 1997) and the semi-direct effect of aerosol radiative and climate forcing (Gu *et al.* 2011). It is important to study these AIEs, not only for gaining insight into the physics of aerosol–cloud interaction but also for the parameterization of initial cloud particle number concentration in global and regional climate modelling study. Quantification of the dust indirect effect in association with clouds is subject to large uncertainties because of our limited understanding of the physical and chemical processes controlling cloud formation in the presence of dust aerosols, particularly in the case of heterogeneous ice nucleation (Cantrell and Heymsfield 2005). There are also uncertainties and difficulties in determining dust AIEs involving clouds by means of *in situ* observations, and global and regional climate model simulations (e.g. Liu and Penner 2005, Lohmann *et al.* 2007).

The full effects of both anthropogenic and naturally occurring mineral dusts on the Earth's climate system have yet to be fully realized and remain the topics of contemporary research. The current assessment of the radiative effects of mineral dust in the working group summary of the Intergovernmental Panel on Climate Change (IPCC) report (Forster *et al.* 2007) reveals large uncertainties in both the magnitude and sign of the direct radiative forcing, primarily due to measurement biases inherent in key dust properties, as well as uncertainties in quantifying competing thermal effects of both longwave and shortwave radiative forcings. Based on the work of previous investigators (e.g. Tegen *et al*. 1996, Hansen *et al.* 1997, Sokolik and Toon 1999), a tentative global annual mean dust radiative forcing in the range -0.6 to $+0.4$ Wm^{-2} was reported with large uncertainties; these stem from model assumptions, lack of observational data and technical difficulties in measurements. Local dust direct radiative forcing during a dust storm event with heavy dust loading could be larger than the global mean by up to two orders of magnitude. In addition to causing climatic perturbations, major dust events can severely reduce near-surface visibility and contribute to a number of problems in military (Miller 2003) and in commercial activities.

At this point, the AIE of the first kind on liquid water clouds coexisting with anthropogenic pollutants, fire smoke and black carbons has been extensively studied from the perspectives of microphysical parameterization, regional and global modelling and satellite observations. For satellite- and ground-based remote-sensing data analyses, Nakajima *et al.* (2001) correlated the column aerosol number concentration and low-cloud microphysical parameters, employing Advanced Very High Resolution Radiometer (AVHRR) data over the ocean for 4 months in 1990. Chameides *et al.* (2002) examined the correlation between the International Satellite Cloud Climatology Project (ISCCP) cloud amount and model-simulated anthropogenic aerosol optical depth. Bréon *et al.* (2002) related the Polarization and Directionality of the Earth's Reflectances (POLDER)-derived cloud particle radius

to aerosol parameters over tropical oceans. Sekiguchi *et al.* (2003) investigated the correlations between aerosol and liquid water cloud parameters derived from global AVHRR and POLDER data sets for evaluating the radiative forcing of AIE. The global statistics showed that the effective particle radius and optical depth of low clouds significantly correlate with the column number concentration of the aerosol particles, indicating an AIE.

With the launch of Terra and Aqua satellites in December 1999 and May 2001, respectively, radiance data collected by the Moderate Resolution Imaging Spectroradiometer (MODIS) onboard both platforms became available for the study of aerosol–cloud indirect effect. Both Terra and Aqua satellites are in Sun-synchronous polar orbits with daytime equator crossings at 10:30 am and 1:30 pm Local Standard Time (LTC), respectively. Aqua is the leading platform of the A-Train. MODIS has a 1 km^2 field of view mapping to a swath of approximately 2330 km. Near complete global coverage is achieved every day, acquiring radiance data using 36 spectral band sensors. Massie *et al.* (2007) analysed MODIS reflectances and aerosol products over India and the Indian Ocean from 2003 to 2005 to study AIEs as a function of cloud-top pressure. Limited analyses have also been conducted using ground-based remote-sensing observations from Raman lidar, microwave radiometer, radar and optical particle counters to quantify the Twomey effect (Feingold *et al.* 2003).

On the other hand, investigation of the dust AIE on ice cloud formation has been limited. Sassen (2002) analysed polarization diversity lidar (PDL) data collected at the Salt Lake City site, showing that dust transported from East Asia to North America did affect ice cloud formation. Sassen *et al.* (2003) and Demott *et al.* (2003) demonstrated similar AIEs for dust particles transported from West Africa to the Caribbean Sea, based on data collected during the Cirrus Regional Study of Tropical Anvils and Cirrus Layers Florida Area Cirrus Experiment (CRYSTAL-FACE) campaign. Chylek *et al.* (2006) obtained a statistically significant correlation between the effective radius ice crystal inferred from MODIS and the level of aerosol loaded during the Indian Ocean Experiment (INDOEX), which suggests a significant aerosol impact on ice clouds. Recently, Min and Li (2010) used the Cloud's and the Earth's Radiant Energy System (CERES) and MODIS data sets to study the long-wave indirect effect of mineral dust on ice clouds, and Lee and Penner (2010) examined the AIE on ice clouds through the use of a cloud-system resolving model.

Ou *et al.* (2009) adopted an alternative approach to investigate these effects through analysis of MODIS cloud and aerosol data products, which contain rich and valuable information that can be used to investigate the relationship between aerosols and cloud formation. They examined the MODIS data covering regions of frequent dust outbreaks in East Asia, the Middle East and West Africa, as well as areas associated with long-range dust transportation such as the equatorial tropical Atlantic Ocean. Statistical analysis has been performed for two aerosol/cloud cases that occurred over West Africa and Korea. For each case, Ou *et al.* (2009) compared the domain-averaged cloud mean effective particle sizes for cloudy regions in proximity with different dust loadings and demonstrated that cloud optical depths are larger and cloud effective particle sizes are smaller over heavier dust loading regions, a result consistent with the hypothesis of Twomey effect. This article expands the scope of the preceding study to include the dust AIE on both coexisting ice and water clouds and over both land and ocean. In this work, using Terra/Aqua-MODIS cloud and aerosol data products, we have developed a new analysis involving dust aerosol properties and their associated indirect effect of the first kind on cloud formation.

2. Analysis of satellite data

To determine the liquid water cloud droplet number concentration (N_w), we assume that the cloud droplet size distribution can be represented by the Gamma function (Liou 1992, p. 188),

$$n(r) = Cr^{(1-3b)/b} \exp(-r/ab), \tag{1}$$

where $a = r_e$ and $b = \upsilon_e$. The parameters r_e and v_e are the effective radius and variance, respectively, and the latter is defined as:

$$v_e = \frac{\int (r - r_e)^2 r^2 n(r) \mathrm{d}r}{r_e^2 \int r^2 n(r) \mathrm{d}r}, \tag{2}$$

and the cloud water content (CWC) for spherical droplets can be expressed as:

$$\mathrm{CWC} = \frac{4\pi\rho_w}{3} \int r^3 n\,(r)\,\mathrm{d}r. \tag{3}$$

By substituting equation (1) into (3), the constant C can then be expressed in terms of CWC. Finally, from the integration of $n(r)$ over the size spectrum, we obtain

$$N_w = k\frac{\tau_c}{r_e^2}, \tag{4}$$

where τ_c is the cloud optical depth and the proportionality constant k is determined from the integration of Gamma functions. Thus, N_w can be computed using MODIS-retrieved τ_c and r_e following equation (4).

The determination of the ice cloud and aerosol number concentrations (N_i and N_a) and the procedure for correlating ice cloud and aerosol properties have been described by Ou *et al.* (2009). The ice cloud number concentration is computed based on the relationship between cloud optical depth and particle size distribution. Likewise, the aerosol number concentration is computed based on the relationship between aerosol optical depth and aerosol size distribution. The procedure for correlating liquid water cloud and dust aerosol properties is similar to that for correlating ice cloud and aerosol properties. Because aerosol optical depth is retrieved for each 10 × 10 pixel sub-grid (roughly 1 km^2), the correlation between aerosol and cloud properties is also done for each 10 × 10 pixel sub-grid. Ou *et al.* (2009) discussed the effects of water vapour absorption/emission, large-scale meteorological drivers and cloud contamination. These effects are minimal in the present analysis because of the usage of window spectral bands, the difference in spatial and temporal scales of microphysical (on the order of microns and seconds) and meteorological (on the order of kilometres and hours) processes and the high spatial resolution of the MODIS instrument, which effectively separates clear and cloudy areas using the MODIS cloud mask program (Ackerman *et al*. 2006, Frey *et al.* 2008).

3. Application to MODIS scenes containing dust and clouds

We have collected and examined MODIS Collection 5 aerosol and cloud data covering regions of East Asia and performed correlation analysis for MODIS scenes containing dust aerosols and clouds. The cloud products (data headings begin with

MOD06/MYD06) that are analysed have been described by King *et al*. (2003) and Platnick *et al.* (2003). In addition, King *et al.* (2006) provided a description of the Collection 5 cloud products. We extracted 'cloud effective radius' and 'cloud phase infrared' for this study. The cloud thermodynamic phase algorithm has been described by King *et al.* (2004). The aerosol products that are analysed have been described by Remer *et al.* (2005) and Levy *et al.* (2007a,b). The Collection 5 aerosol products that are analysed in this study have been described by Levy *et al.* (2010). A number of interesting MODIS dust scenes have been identified in order to study the Twomey effect of dust aerosols on clouds.

We have correlated cloud and aerosol parameters by means of statistical analysis and interpreted resulting correlation trends based on the physical principles governing cloud microphysics. Throughout the study, we have divided the identified aerosol or ice-cloud scene into 10×10 km sub-grids to correlate ice and aerosol properties. Because the MODIS cloud mask identifies a pixel as either clear/aerosol or cloud and because the current MODIS detection/retrieval algorithms cannot simultaneously detect or retrieve aerosol and cloud parameters on a pixel-by-pixel basis, correlation analysis was performed by using the average aerosol and cloud properties within each sub-grid that contains both ice cloud and aerosol pixels. This is a novel approach, which is the central theme of this study. We present three case studies demonstrating significant dust-cloud indirect effect for both ice and water clouds below.

3.1 *Qualitative and quantitative study of dust AIE (8 April 2006 at 0440 UTC)*

Figure 1(*a*) shows a Terra/MODIS scene for 8 April 2006 at 0440 UTC over Northeast Asia. This scene contains a significant presence of original and transported dust layers with imbedded clouds. We selected three domains for this study. We first investigated the AIE by the comparison of aerosol optical depths and cloud effective particle sizes for cloudy regions with different dust loadings. To the best of our physical understanding, clouds over an area of heavier dust loading, presumably with many of the dust particles serving as potential CCN or IN, would probably be affected more than clouds over a lighter dust region.

Over both the Eastern Siberia (domain A) and Inner Mongolia (domain B) regions, the non-zero values of 1.38 μm and reflectance and the low cloud-top temperature (T_c) values (<243 K) for both regions further confirm that both domains contain cirrus clouds. In addition, the MODIS cloud mask shows that both areas are masked by cloudiness, and the cloud-phase mask indicates that parts of the cloudiness within both regions are ice clouds. A list of parameters and their mean values for domains A and B is given in table 1. For domain A, τ_a varies between 0.9 and 1.8 (figure 1(*b*)) with a mean value of 1.2, whereas r_e varies between 5 and 35 μm, with a mean value of 17.3 μm (figure 1(*c*)). For domain B, we determined τ_a in the range 0–0.9 (figure 1(*b*)), with a mean value of 0.28, and r_e in the range 5–80 μm (figure 1(*c*)), with a mean value of 23.8 μm. It is evident that for domain A, the dust optical depth is larger, but at the same time the cloud particle size is smaller, consistent with the Twomey effect for aerosol–water cloud interactions.

Subsequently, we investigated the dust indirect effect on liquid water clouds with a strong dust loading. Here, we analysed the same Aqua/MODIS scene for 8 April 2006 at 0440 UTC over the Eastern Asian continent and surrounding oceans, as shown in figure 1, to demonstrate the presence of strong dust AIE with heavier dust loadings, more correlation sub-grid points and higher correlation coefficients than those shown by Ou *et al.* (2009). Over Japan (domain C), there was a distinct presence of

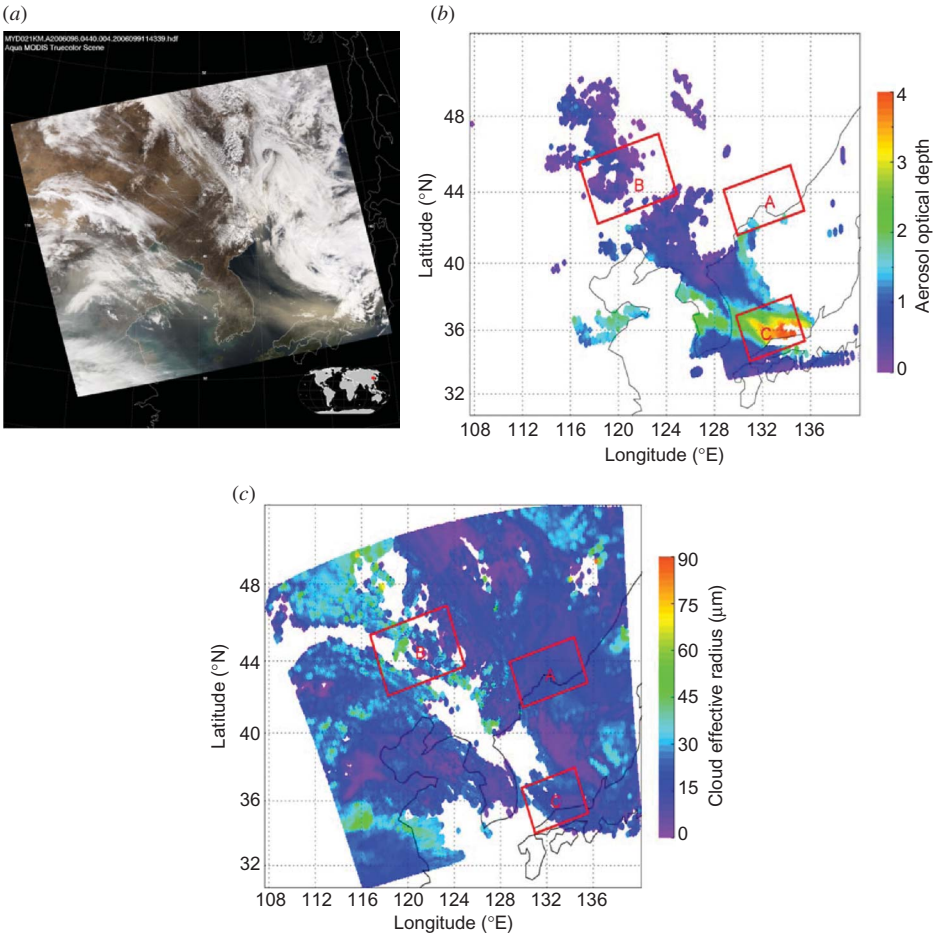

Figure 1. MODIS scene with simultaneous presence of cirrus clouds and dust layers. Images for the MODIS overpass on 8 April 2006 at 0440 UTC over the Northeast Asian continent, Korea and Japan: (*a*) RGB, (*b*) aerosol optical depth and (*c*) cloud effective particle size. Domains A, B and C are areas of dust layers with imbedded clouds.

Table 1. Parameter ranges and their mean values for domains A and B of the MODIS scene for 8 April 2006 at 0440 UTC over Northeast Asia.

	Parameter range (mean value)		
Domain	τ_c	r_e (μm)	τ_a
A	0–50 (10.9)	5–35 (17.3)	0.9–1.8 (1.20)
B	0–60 (6.7)	5–80 (23.8)	0–0.9 (0.28)

heavy aerosol loading mixed with water clouds. Figures 2(*a*)–(*d*) display the correlation between τ_c and τ_a, r_e and τ_a, IWP and τ_a, and N_w and N_a, where IWP is the ice water path. The dust loading is heavy ($\tau_{a,max} = 4$), the range of τ_a is wider than those shown by Ou *et al.* (2009) (($\tau_{a,max} - \tau_{a,min}$) = 3.5) and the number of sub-grids available

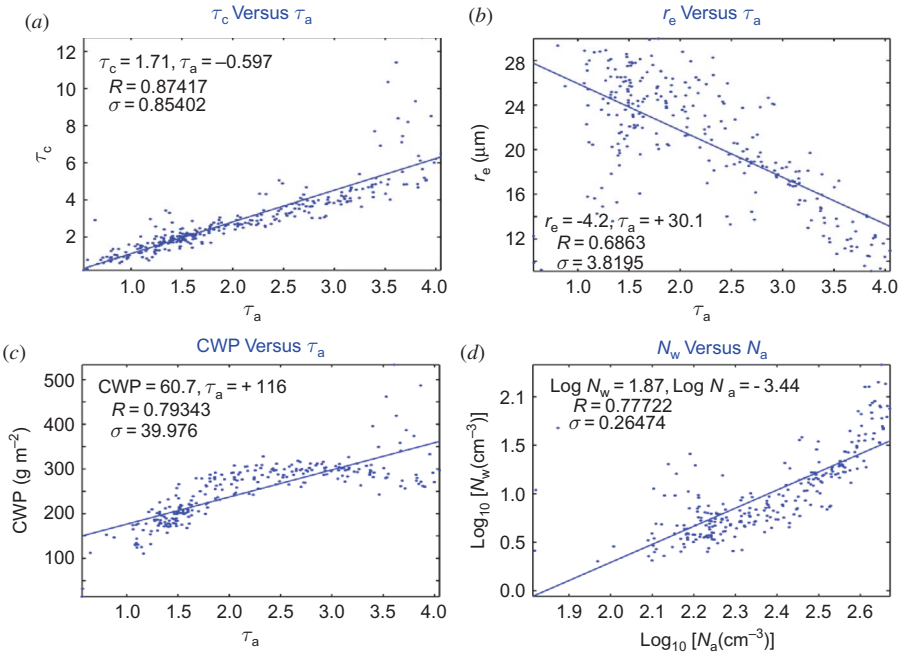

Figure 2. Correlations between water cloud and dust aerosol properties over Japan on 8 April 2006 at 0440 UTC: (*a*) τ_c versus τ_a, (*b*) r_e versus τ_a, (*c*) cloud water path (CWP) versus τ_a and (*d*) cloud droplet number concentration N_w versus aerosol number concentration N_a. The straight lines denote linear fittings of the data points, with the fitting equation given in each frame.

for correlation studies with coexisting dust and clouds is 306. All correlation coefficients are larger than 0.6, indicating strong relationships between cloud and aerosol parameters. The cloud optical depth τ_c varies between 0.5 and 12 and is shown to increase almost linearly with τ_a. For each correlation data point, τ_c is mostly larger than τ_a, particularly for τ_a near the maximum value. The cloud water path varies between 250 and 300 g m^{-2}, approximately satisfying the requirement of constant cloud water content for the study of AIE.

The cloud effective radius r_e, varying between 9 and 30 μm, is negatively correlated with τ_a, and the dust AIE on water clouds is clearly demonstrated in this case. The slopes $\Delta\tau_c/\Delta\tau_a$, $\Delta r_e/\Delta\tau_a$, $\Delta\mathrm{IWP}/\Delta\tau_a$ and $\Delta\log(N_w)/\Delta\log(N_a)$ are 1.7, −4.2 μm, 6.5 g m^{-2} and 1.87, respectively. The estimated AIE index, defined as the partial derivative $\partial[\log(r_e)]/\partial[\Delta\log(\tau_a)]$ (Feingold *et al.* 2003) is 0.5, based on the estimated domain-mean value of r_e and τ_a (∼21 μm and ∼2.5). This AIE index is larger than the maximum value of 0.33 for spherical water droplets, based on the assumption of constant cloud water content, indicating a strong dust AIE on water clouds.

Correlations of r_e versus τ_a and of $\log(N_w)$ versus $\log(N_a)$ are further compared with those presented by Nakajima *et al.* (2001), who analysed global AVHRR data for four seasonal representative months (January, April, July and October) in 1990. In their figure 5, they showed that for all four seasons, r_e is negatively correlated with $\log(N'_a)$ and that $\log(N'_w)$ is positively correlated with $\log(N'_a)$, where N'_a and N'_w are vertically integrated values of N_a and N_w, using the following approximations $N'_a = N_a\Delta z_a$ and $N'_w = N_w\Delta z_c$, where Δz_a and Δz_c are the thicknesses of aerosol and

cloud layers, respectively. We find that $\Delta\log(N_w)/\Delta\log(N_a) = \Delta\log(N'_w)/\Delta\log(N'_a)$. Based on the formulations derived by Ou *et al.* (2009), $\tau_a = 2\pi r_a^2 N'_a$, where r_a is prescribed as 0.5 μm, we estimated the slope value of $\Delta r_e/\Delta\tau_a = -1.1$ μm and $\Delta\log(N_w)/\Delta\log(N_a) = 0.45$. By comparison, the magnitudes of two slope values shown in figure 2 are much larger. Note that Nakajima *et al.* (2001) derived globally averaged values, which include all types and densities of aerosols, whereas the current case is an extreme example of heavy dust loading. The results illustrate additional evidence that dust aerosols and water cloud properties are highly correlated and that the dust indirect effect on cloud formation can be detected and reasonably quantified on the basis of satellite observations.

3.2 *Comparison of dust indirect effect on ice and liquid water clouds (10 March 2006 at 0510 UTC)*

Figure 3(*a*) shows an Aqua/MODIS scene for 10 March 2006 at 0510 UTC over Northeast Asia. Similarly to the scene shown in figure 1, this case contains a significant presence of original and transported dust layers with imbedded clouds over the Yellow Sea, Northeastern China and North Korea. We selected a domain within which both ice and liquid water clouds were present over the portion of the Yellow Sea between the Shang-dong and Liao-Ning Peninsulas. Based on cloud-phase mask results, this domain exhibits a heavy dust loading, and liquid water clouds were mixed with scattered ice clouds. Over ice cloud pixels, 1.38 μm band reflectances are non-zero and T_c(<243 K) is low. In addition, the MODIS cloud mask shows that areas masked by clear and cloudiness are collocated with negative and positive brightness temperature differences between 11 and 12 micron band (BTD11-12) values, respectively (Hansell *et al.* 2007). Figure 3(*b*) displays a τ_a map, where its value is as high as 6. Figure 3(*c*) shows the distribution of r_e. Within the selected domain, r_e is between 5 and 30 μm.

Figures 4(*a*)–(*d*) display the correlation between τ_c and τ_a, r_e and τ_a, IWP and τ_a and N_i and N_a for ice cloud pixels. This case is also statistically significant and is characterized by heavy dust loading ($\tau_{a,max} = 4.7$), a wide range of τ_a (($\tau_{a,max} - \tau_{a,min}$) = 4.5) and a large number of correlation sub-grids (136). The correlation coefficients for τ_c and τ_a, r_e and τ_a and N_i and N_a are generally larger than 0.6, indicating strong relationships between cloud and aerosol parameters. The cloud optical depth τ_c varies between 0.7 and 5.5 and is shown to increase with increasing τ_a. For each correlation data point, τ_c is generally larger than τ_a, particularly for $\tau_a > 3$. The cloud effective particle size r_e varies between 10 and 27 μm and decreases with increasing τ_a. The IWP varies between 250 and 300 g m^{-2}, which is weakly correlated with τ_a with a correlation coefficient of 0.37. The slopes $\Delta\tau_c/\Delta\tau_a$, $\Delta r_e/\Delta\tau_a$, ΔIWP$/\Delta\tau_a$ and $\Delta\log(N_i)/\Delta\log(N_a)$ are 0.949, −3.73 μm, 2.83 g m^{-2} and 0.328, respectively. The estimated aerosol AIE index is 0.47 based on estimated domain-mean values of r_e and τ_a (∼20 μm and ∼2.5).

Figures 4(*e*)–(*h*) illustrate the same correlations between cloud and aerosol parameters for water cloud pixels. This is another statistically significant case with heavy dust loading ($\tau_{a,max} = 5$), revealing a wide range of τ_a and a large number of correlation sub-grids (473). The correlation coefficients for τ_c and τ_a, r_e and τ_a, IWP and τ_a and N_i and N_a are generally larger than 0.75, indicating a strong relationship between cloud and aerosol parameters. The cloud optical depth τ_c varies between 0.2 and 5.5 and increases with increasing τ_a. On the contrary, the cloud effective particle size r_e, which varies between 5 and 28 μm, decreases with increasing τ_a. CWP varies

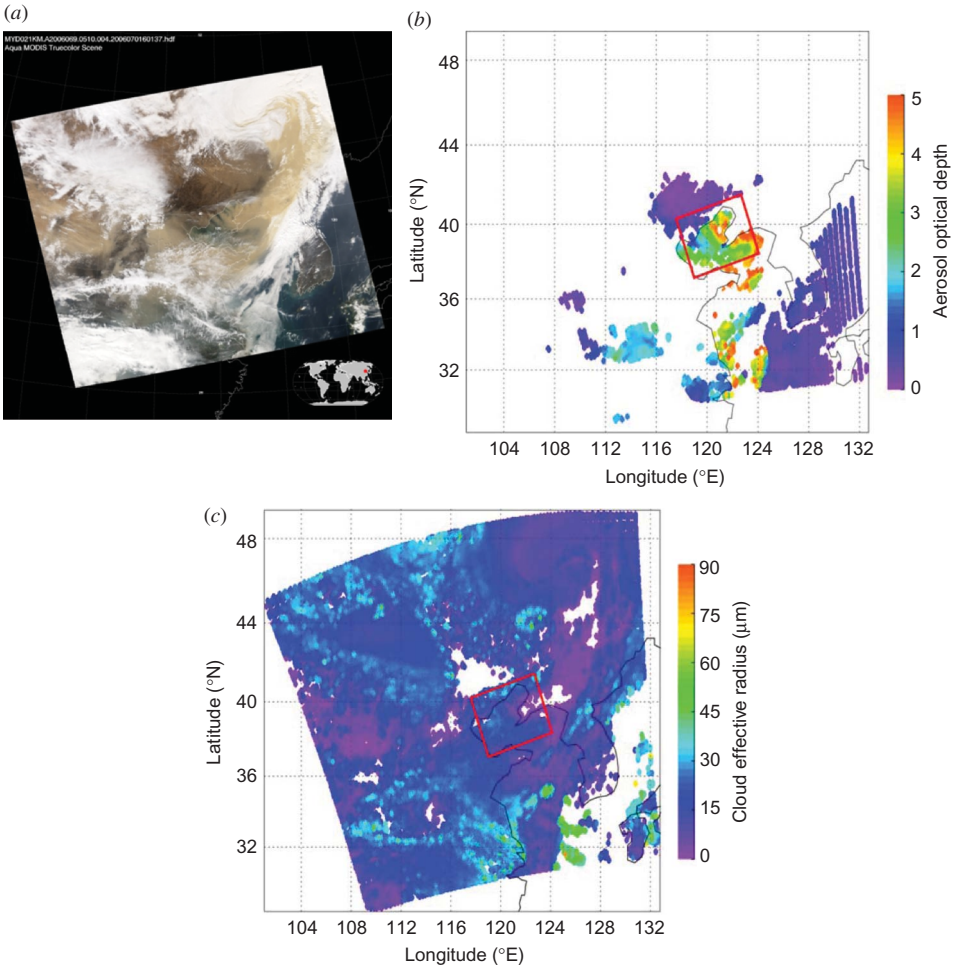

Figure 3. Same as figure 1, except for the MODIS overpass on 10 March 2006 at 0510 UTC over the Northeast Asian continent and Korea. The rectangular domain contains dust layers with imbedded clouds.

between 10 and 300 g m^{-2} and is weakly correlated with τ_a with a correlation coefficient of 0.27. The slopes $\Delta\tau_c/\Delta\tau_a$, $\Delta r_e/\Delta\tau_a$, $\Delta IWP/\Delta\tau_a$ and $\Delta\log(N_i)/\Delta\log(N_a)$ are 0.988, −4.26 μm, 13.9 g m^{-2} and 1.65, respectively. The estimated aerosol AIE index is 0.75 based on the estimated domain-mean value of $r_e(\sim 17)$ and $\tau_a(\sim 3)$. This AIE index is again larger than the maximum theoretical value of 0.33 derived for spherical water droplets, indicating a strong dust AIE on water clouds.

3.3 *Comparison of dust indirect effects over land and ocean (31 March 2007 at 0500 UTC)*

Figure 5(*a*) shows another Aqua/MODIS scene for 31 March 2007 at 0500 UTC over Northeastern and Eastern China and the East China Sea. Similarly to the scenes shown in figures 1 and 3, this case contains a significant presence of dust layers mixed with clouds. Over Northeastern China, BTD11-12 values are around −4 K, indicating

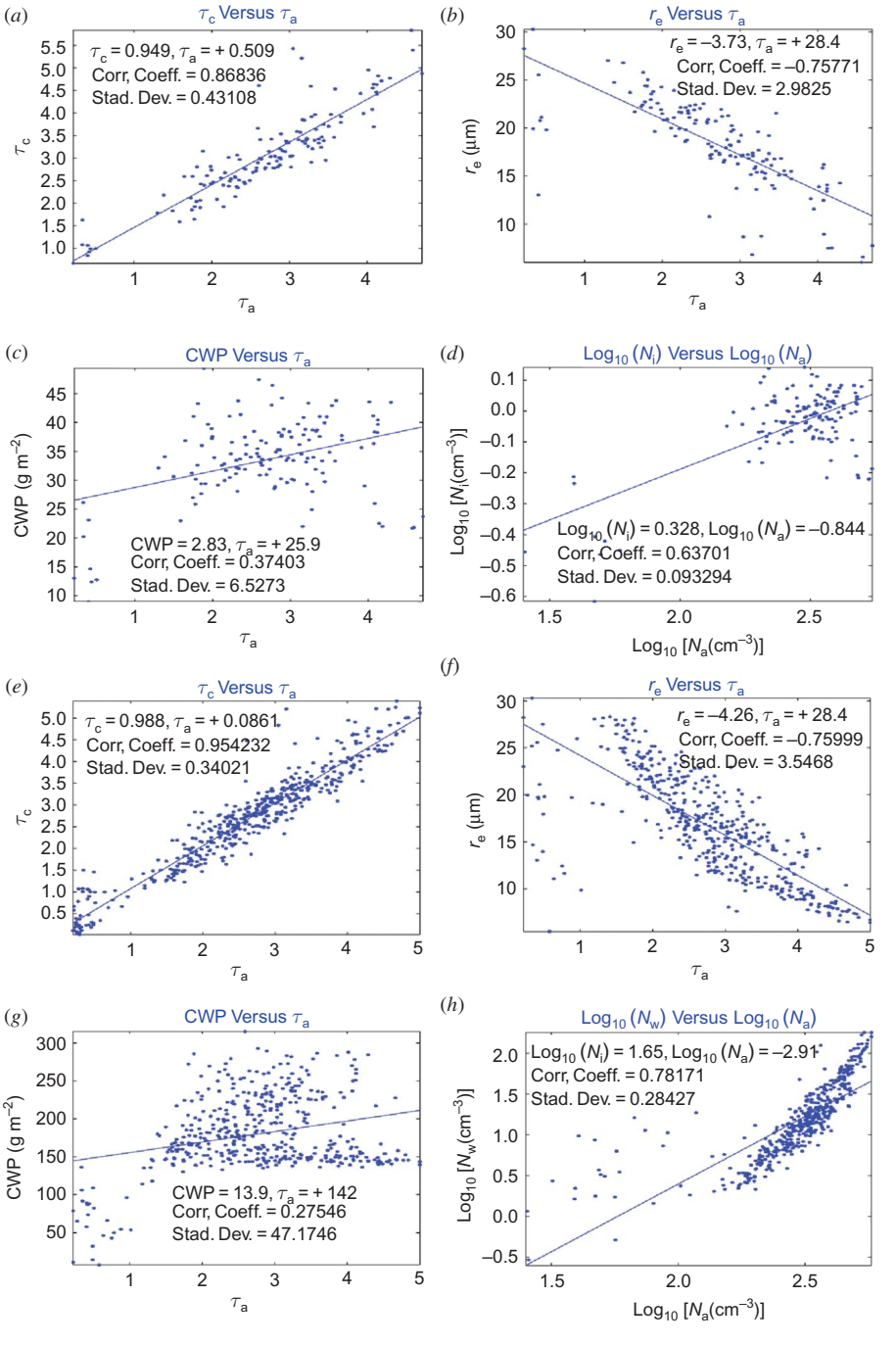

Figure 4. (*a*)–(*d*) Same as figure 2, except for correlations of the dust aerosol and ice cloud properties on 10 March 2006 at 0510 UTC. Figures (*e*)–(*h*) are the same as figures (*a*)–(*d*), except for correlations of the dust aerosol and water cloud properties.

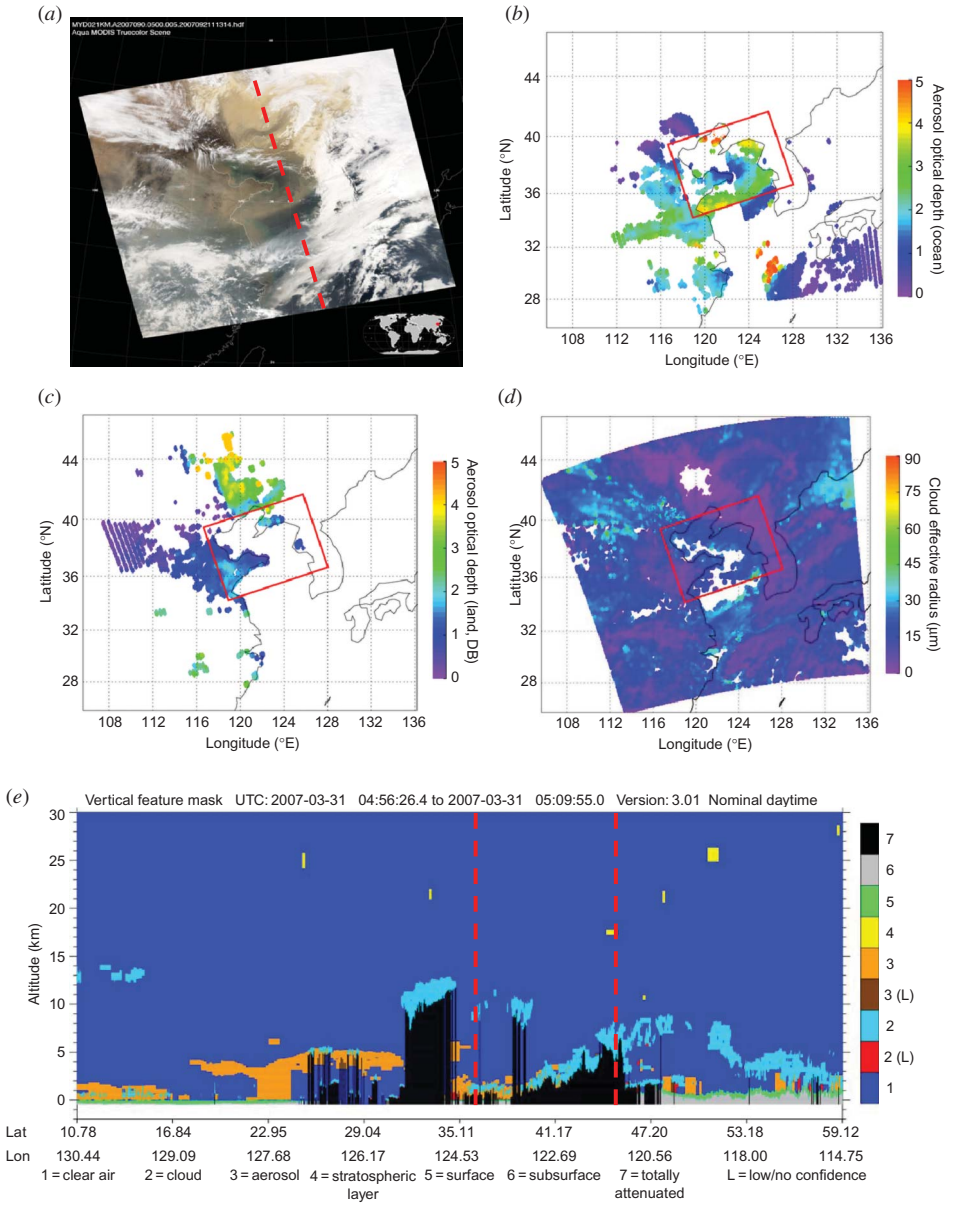

Figure 5. Images for the MODIS overpass on 31 March 2007 at 0500 UTC over Northeastern and Eastern China and the East China Sea; (*a*) RGB; (*b*) aerosol optical depths over ocean; (*c*) aerosol optical depths over land; and (*d*) cloud effective particle sizes. The rectangular domain contains dust over both land and water with imbedded clouds; (*e*) result of the vertical feature mask obtained from CALIOP-polarized echoes. Between the two vertical dashed lines, which denote the southern and northern bounds of the selected domain, clouds mixed with dust have been identified using the lidar depolarization technique.

a heavy load of dust aerosols. Major cirrus clouds were present over Northeastern China, Mongolia and Southern Japan, where the 1.38 μm band reflectances are larger than 0.1, whereas T_c are lower than 243 K. The cloudy areas are mostly liquid water

clouds. The distributions of cirrus and liquid water clouds are consistent with cloud-phase mask results. In addition, the MODIS cloud mask illustrates that the areas masked by clear and cloudiness are collocated with negative and positive BTD11-12 values, respectively. Figures 5(*b*) and (*c*) display aerosol optical depth maps over ocean and land, respectively, where the results over land were obtained by the Deep Blue algorithm developed by Hsu *et al.* (2004). We selected a domain within which dust aerosols are present over both ocean and land such that both ice and liquid water clouds were present over Northeastern China and the East China Sea. Dust aerosols over ocean and land were located in the southern and northern halves of the selected domain. In figure 5(*d*), we see that $r_e < 10$ μm for cirrus clouds (cyan coloured) and $r_e < 10$ μm for water clouds (deep-blue coloured). The result of the vertical feature mask derived from polarized echoes of the Cloud-Aerosol Lidar with Orthogonal Polarization (CALIOP) onboard the Cloud-Aerosol Lidar and Infrared Pathfinder Satellite Observations (CALIPSO) satellite is shown in figure 5(*e*). Between the two vertical dashed lines, which denote the southern and northern bounds of the selected domain, clouds (cyan coloured) and dust layers (orange coloured) have been identified using the lidar depolarization technique. This image clearly demonstrates that clouds and dust were in the same atmospheric layers, which extended to 5 km.

Figures 6(*a*)–(*d*) display the correlation between τ_c and τ_a, r_e and τ_a, IWP and τ_a and N_i and N_a for ice cloud pixels over ocean. As in figures 2 and 4, the dust loading is heavy ($\tau_{a,max} = 5$), with 251 sub-grids available for correlation studies. The correlation coefficients between τ_c and τ_a, and r_e and τ_a, are larger than 0.6, indicating strong relationships between cloud and aerosol parameters. The cloud optical depth τ_c varies between 1 and 8 and is shown to have a linearly increasing trend as a function of τ_a. For each correlation data point, τ_c is mostly larger than τ_a. The slopes $\Delta\tau_c/\Delta\tau_a$, $\Delta r_e/\Delta\tau_a$, $\Delta\text{IWP}/\Delta\tau_a$ and $\Delta\log(N_i)/\Delta\log(N_a)$ are 0.758, −3.51 μm, 1.72 g m^{-2} and 0.568, respectively. Based on the estimated domain-mean value of r_e(∼20 μm) and τ_a (∼2.5), we determined an aerosol AIE index of 0.44.

Figures 6(*e*)–(*h*) illustrate the same correlations between cloud and aerosol parameters as in figures 6(*a*)–(*d*), but for ice cloud pixels over land. The dust loading is heavy ($\tau_{a,max} = 4$), with 339 sub-grids available for correlation studies. The correlation coefficients between τ_c and τ_a, and r_e and τ_a, are similar to those presented in figures 6(*a*)–(*d*). Based on the estimated domain-mean value of r_e (∼8 μm) and τ_a (∼2), we derived an aerosol AIE index of 0.52.

For the same τ_a, the cloud effective particle radius r_e over land is much smaller than over ocean, a result consistent with previous studies. For this reason, the cloud optical depth τ_c over land is much larger than over ocean, which is associated with a stronger scattering contribution. However, AIE is slightly stronger over land than over ocean.

4. Concluding remarks

This study addresses the AIE of the first kind on ice and liquid water cloud formation over both land and ocean by analysing pertinent data from Terra/Aqua/MODIS over East Asia. The focus of our analysis is to examine the variability in correlation between cloud parameters and tropospheric dust parameters inferred from the available satellite cloud and aerosol data results. We selected and collected suitable aerosol/cloud scenes, identified regions for analysis, statistically correlated ice cloud and aerosol parameters and interpreted resulting correlation trends based on physical principles.

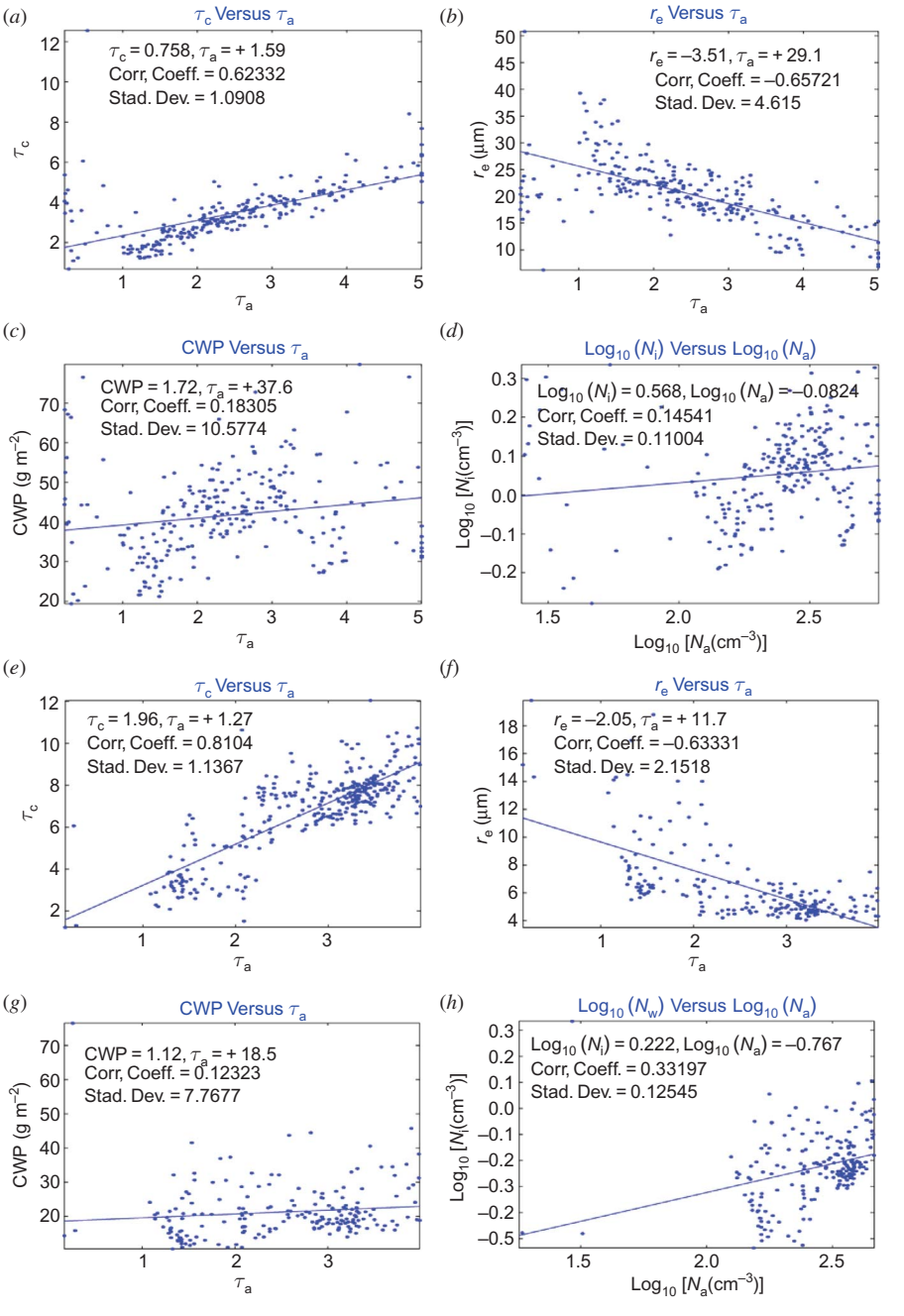

Figure 6. (*a*)–(*d*) Same as figure 2, except for correlations of dust aerosol and ice cloud properties on 31 March 2007 at 0510 UTC for ice cloud pixels over ocean within the selected domain shown in figure 5; figures (*e*)–(*h*) are the same as figures (*a*)–(*d*), except for correlations of dust aerosol and ice cloud properties for ice cloud pixels over land.

We first demonstrated that the dust indirect effect on cirrus clouds can be detected and reasonably quantified by satellite observations. Using a number of carefully selected cases, we further showed that ice cloud mean effective particle sizes decrease with increasing dust aerosol optical depth for a range of different dust loadings, clearly illustrating the Twomey effect for dust–ice cloud interactions.

Second, based on the investigation of three MODIS scenes and the analysis of correlations of dust and cloud properties, we showed the strong AIE within the selected domains involving heavy dust coexisting with liquid water and ice clouds. We investigated the dust indirect effect on liquid water clouds with a strong dust loading. We demonstrated that there is a strong correlation between dust and liquid water cloud parameters. Subsequently, we compared the dust indirect effect on ice and water clouds. For the selected domain, which contained a dust layer mixed with both ice and water clouds, a negative correlation between τ_a and r_e for both ice and water clouds was derived. The correlation coefficients for τ_c and τ_a, r_e and τ_a and N_i and N_a were all larger than 0.6, whereas the correlations between dust and water cloud properties were better than those between dust and ice cloud properties.

Finally, we compared dust indirect effects on ice clouds over land and over ocean. Aqua/MODIS scenes over Northeastern and Eastern China, and the East China Sea, were selected, which contained dust layer and ice clouds over land and over ocean. We showed that there is a negative correlation between τ_a and r_e for ice clouds. The correlation coefficients for τ_c and τ_a and r_e and τ_a are larger than 0.6, whereas the correlations between dust and ice cloud properties over land and over water are comparable, although r_e values over land are much smaller than those over ocean. The preceding results illustrate evidence of dust and cloud interactions over Eastern Asia consistent with the hypothesis of the Twomey effect.

Acknowledgement

This work was supported in part by the NASA/Goddard Grant NNX09AR42G.

References

Ackerman, S., Strabala, K., Menzel, P., Frey, R., Moeller, C., Gumley, L., Baum, B., Schaaf, C. and Riggs G., 2006, *Discriminating Clear-Sky from Clouds with MODIS Algorithm Theoretical Basis Document (MOD35)*, Version 5.0, 112 pp. (Greenbelt, MD: Goddard Space Flight Center). Available online at: http://modis-atmos.gsfc.nasa.gov/_docs/atbd_mod06.pdf

Albrecht, B.A., 1989, Aerosols, cloud microphysics, and fractional cloudiness. *Science*, **245**, pp. 1227–1230.

Bréon, F.-M., Tanré, D. and Generoso, S., 2002, Aerosol effect on cloud droplet size monitored from satellite. *Science*, **295**, pp. 834–838.

Cantrell, W. and Heymsfield, A.J., 2005, Production of ice in tropospheric clouds: a review. *Bulletin of the American Meteorological Society*, **86**, pp. 795–807.

Chameides, W.L., Lou, C., Saylor, R., Streets, D., Huang, Y., Bergin, M. and Giorgi, F., 2002, Correlation between model-calculated anthropogenic aerosols and satellite-derived cloud optical depths: indication of indirect effect? *Journal of Geophysical Research*, **107**, 4085, doi:10.1029/JD000208.

Chylek, P., Dubey, M.K., Lohmann, U., Ramanathan, V., Kaufman, Y.J., Lesins, G., Hudson, J., Altmann, G. and Olsen, S., 2006, Aerosol indirect effect over the Indian Ocean. *Geophysical Research Letters*, **33**, L06806, doi:10.1029/2005GL025397.

DeMott, P.J., Sassen, K., Poellot, M.R., Baumgardner, D., Rogers, D.C., Brooks, S., Prenni, A.J. and Kreidenweis, S.M., 2003, African dust aerosols as atmospheric ice nuclei. *Geophysical Research Letters*, **30**, 1732, doi:10.1029/2003GL017410.

Feingold, G., Eberhard, W.L., Veron, D.E. and Previdi, M., 2003, First measurements of the Twomey indirect effect using ground-based remote sensors. *Geophysical Research Letters*, **30**, 1287, doi:10.1029/2002GL016633.

Forster, P., Ramaswamy, V., Artaxo, P., Berntsen, T., Betts, R., Fahey, D.W., Haywood, J., Lean, J., Lowe, D.C., Myhre, G., Nganga, J., Prinn, R., Raga, G., Schulz, M. and Van Dorland, R., 2007, Changes in atmospheric constituents and in radiative forcing. In *Climate Change 2007: The Physical Science Basis. Contribution of Working Group I to the Fourth Assessment Report of the Intergovernmental Panel on Climate Change*, S. Solomon, D. Qin, M. Manning, Z. Chen, M. Marquis, K.B. Averyt, M. Tignor and H.L. Miller (Eds.) (Cambridge and New York: Cambridge University Press).

Frey, R.A., Ackerman, S.A., Liu, Y.H., Strabala, K.I., Zhang, H., Key, J.R. and Wang, X.G., 2008, Cloud detection with MODIS. Part I: improvements in the MODIS cloud mask for collection 5. *Journal of Atmospheric and Oceanic Technology*, **25**, pp. 1057–1072.

Grassl, H., 1979, Possible changes of planetary albedo due to aerosol particles. In *Man's Impact on Climate*, W. Bach, J. Pankrath and W. Kellogg (Eds.) (New York: Elsevier).

Gu, Y., Liou, K.N., Ou, S.C. and Fovell, R., 2011, Cirrus cloud simulations using WRF with improved radiation parameterization and increased vertical resolution. *Journal of Geophysical Research*, **116**, D06119, doi:10.1029/2010JD014574.

Hansell, R.A., Ou, S.C., Liou, K.N., Roskovensky, J.K., Tsay, S.C., Hsu, C. and Ji, Q., 2007, Simultaneous detection/separation of mineral dust and clouds using MODIS Infrared window data. *Geophysical Research Letters*, **34**, L11808, doi:10.1029/2007GL029388.

Hansen, J., Sato, M. and Ruedy, R., 1997, Radiative forcing and climate response. *Journal of Geophysical Research*, **102**, pp. 6831–6864.

Hsu, N.C., Tsay, S.-C., King, M.D. and Herman, J.R., 2004, Aerosol properties over bright-reflecting source regions. *IEEE Transactions on Geoscience and Remote Sensing*, **42**, pp. 557–569.

King, M.D., Menzel, W.P., Kaufman, Y.J., Tanré, D., Gao, B.C., Platnick, S., Ackerman, S.A., Remer, L.A., Pincus, R. and Hubanks, P.A., 2003, Cloud and aerosol properties, precipitable water, and profiles of temperature and humidity from MODIS. *IEEE Transactions on Geoscience and Remote Sensing*, **41**, pp. 442–458.

King, M.D., Platnick, S., Hubanks, P.A., Arnold, G.T., Moody, E.G., Wind, G. and Wind, B., 2006, *Collection 005 Change Summary for the MODIS Cloud Optical Property (06_OD) Algorithm*. Available online at: http://modis-atmos.gsfc.nasa.gov/C005_Changes/C005_CloudOpticalProperties_ver311.pdf

King, M.D., Platnick, S., Yang, P., Arnold, G.T., Gray, M.A., Riedi, J.C., Ackerman, S.A. and Liou, K.-N., 2004, Remote sensing of liquid water and ice cloud optical thickness and effective radius in the arctic: application of airborne multispectral MAS data. *Journal of Atmospheric and Oceanic Technology*, **21**, pp. 857–875.

Lee, S.S. and Penner, J.E., 2010, Aerosol effects on ice clouds: can the traditional concept of aerosol indirect effects be applied to aerosol–cloud interactions in cirrus clouds? *Atmospheric Chemistry and Physics*, **10**, pp. 10345–10358.

Levy, R., Remer, L. and Dubovik, O., 2007a, Global aerosol optical properties and application to Moderate Resolution Imaging Spectroradiometer aerosol retrieval over land. *Journal of Geophysical Research – Atmospheres*, **112**, D13210, doi:10.1029/2006JD0078151.

Levy, R., Remer, L., Mattoo, S., Vermote, E. and Kaufman, Y.J., 2007b, Second-generation operational algorithm: retrieval of aerosol properties over land from inversion of Moderate Resolution Imaging Spectroradiometer spectral reflectance. *Journal of Geophysical Research – Atmospheres*, **112**, D13211, doi:10.1029/2006JD 007811.

Levy, R.C., Remer, L.A., Kleidman, R.G., Mattoo, S., Ichoku, C., Kahn, R. and Eck, T.F., 2010, Global evaluation of the Collection 5 MODIS dark-target aerosol products over land. *Atmospheric Chemistry and Physics*, **10**, pp. 10399–10420.

Liou, K.N., 1992, *Radiation and Cloud Processes in the Atmosphere: Theory, Observation, and Modeling*, 487 pp. (New York: Oxford University Press) [Description and Reviews].

Liou, K.N. and Ou, S.C., 1989, The role of cloud microphysical processes in climate: an assessment from a one-dimensional perspective. *Journal of Geophysical Research*, **94**, pp. 8599–8607.

Liu, X. and Penner, J.E., 2005, Ice nucleation parameterization for global models. *Meteorologische Zeitschrift*, **14**, pp. 499–514.

Lohmann, U., Quaas, J., Kinne, S. and Feichter, J., 2007, Different approaches for constraining global climate models of the anthropogenic indirect aerosol effect. *Bulletin of the American Meteorological Society*, **88**, pp. 243–249.

Massie, S.T., Heymsfield, A., Schmitt, C. and Muller, D., 2007, Aerosol indirect effects as a function of cloud top pressure. *Journal of Geophysical Research*, **112**, D06202, doi:10.1029/2006JD007383.

Miller, S.D., 2003, A consolidated technique for enhancing desert dust storms with MODIS. *Geophysical Research Letters*, **30**, 2071, doi:10.1029/2003GL018279.

Min, Q. and Li, R., 2010, Long-wave indirect effect of mineral dusts on ice clouds. *Atmospheric Chemistry and Physics*, **10**, pp. 7753–7761.

Nakajima, T., Higurashi, A., Kawamoto, K. and Penner, J.E., 2001, A possible correlation between satellite-derived cloud and aerosol microphysical parameters. *Geophysical Research Letters*, **28**, pp. 1171–1174.

Ou, S.C., Liou, K.N., Wang, X., Hansell, R., Lefevre, R. and Cocks, S., 2009, Satellite remote sensing of dust aerosol indirect effects on ice cloud formation. *Applied Optics*, **48**, pp. 633–647.

Platnick, S., King, M.D., Ackerman, S.A., Menzel, W.P., Baum, B.A., Riedi, J.C. and Frey, R.A., 2003, The MODIS cloud products: algorithms and examples from Terra. *IEEE Transactions on Geoscience and Remote Sensing*, **41**, pp. 459–473.

Remer, L., Kaufman, Y., Tanre, D., Mattoo, S., Chu, D., Martins, J., Li, R., Ichoku, C., Levy, R., Kleidman, R., Eck, T., Vermote, E. and Holben, B.N., 2005, The MODIS aerosol algorithm, products, and validation. *Journal of the Atmospheric Sciences*, **62**, pp. 947–973.

Sassen, K., 2002, Indirect climate forcing over the Western US from Asian dust storms. *Geophysical Research Letters*, **29**, 1465, doi:10.1029/2001GL014051.

Sassen, K., DeMott, P.J., Prospero, J.M. and Poellot, M.R., 2003, Saharan dust storms and indirect aerosol effects on clouds: CRYSTAL-FACE results. *Geophysical Research Letters*, **30**, 1633, doi:10.1029/2003GL017371.

Sekiguchi, M., Nakajima, T., Suzuki, K., Kawamoto, K., Higurashi, A., Rosenfeld, D., Sano, I. and Mukai, S., 2003, A study of the direct and indirect effects of aerosols using global satellite data sets of aerosol and cloud parameters. *Journal of Geophysical Research*, **108**, 4699, doi:10.1029/2002JD003359.

Sokolik, I.N. and Toon, O.B., 1999, Incorporation of mineralogical composition into models of the radiative properties of mineral aerosols from UV to IR wavelengths. *Journal of Geophysical Research*, **104**, pp. 9423–9444.

Tegen, I., Lacis, A.A. and Fung, I., 1996, The influence on climate forcing on mineral aerosols from disturbed soils. *Nature*, **380**, pp. 419–422.

Twomey, S., 1977, The influence of pollution on the shortwave albedo of clouds. *Journal of the Atmospheric Sciences*, **34**, pp. 1149–1152.